Received: 27 August 2020 | Accepted: 18 January 2021

DOI: 10.1002/env.2673

INVITED ARTICLE

WILEY

Effects of corona virus disease-19 control measures on air quality in North China

Xiangyu Zheng[1] | **Bin Guo**[2,3] | **Jing He**[3] | **Song Xi Chen**[1,4]

[1]Guanghua School of Management, Peking University, Beijing, P.R. China

[2]Center of Statistical Research, Southwestern University of Finance and Economics, Chengdu, P.R. China

[3]School of Statistics, Southwestern University of Finance and Economics, Chengdu, P.R. China

[4]Center for Statistical Science, Peking University, Beijing, P.R. China

Correspondence
Song Xi Chen, Guanghua School of Management, Peking University, Beijing 100871, P.R. China.
Email: songxichen@pku.edu.cn

Funding information
China's National Key Research Special Program, Grant/Award Numbers: 2016YFC0207701, 2016YFC0207702; Fundamental Research Funds for the Central Universities, Grant/Award Number: JBK1806002, JBK2102008; National Natural Science Foundation of China Grants, Grant/Award Numbers: 11701466, 11971390, 92046021, 12026607, 71973005, 71991472

Abstract

Corona virus disease-19 (COVID-19) has substantially reduced human activities and the associated anthropogenic emissions. This study quantifies the effects of COVID-19 control measures on six major air pollutants over 68 cities in North China by a Difference in Relative-Difference method that allows estimation of the COVID-19 effects while taking account of the general annual air quality trends, temporal and meteorological variations, and the spring festival effects. Significant COVID-19 effects on all six major air pollutants are found, with NO_2 having the largest decline (−39.6%), followed by $PM_{2.5}$ (−30.9%), O_3 (−16.3%), PM_{10} (−14.3%), CO (−13.9%), and the least in SO_2 (−10.0%), which shows the achievability of air quality improvement by a large reduction in anthropogenic emissions. The heterogeneity of effects among the six pollutants and different regions can be partly explained by coal consumption and industrial output data.

KEYWORDS

difference in relative-difference method, meteorological adjustment, treatment effects estimation

1 | INTRODUCTION

Corona virus disease-19 (COVID-19) has brought many countries' economies and people's ways of life to a stand-still during the pandemic due to the implementation of COVID-19 control measures. As these measures are unprecedentedly wide-spread and over a prolonged period, they have largely curtailed human activities and emission profiles, and created an opportunity to evaluate the effects of emission reduction measures implemented over a large area over an extended time period. The evaluation for the COVID-19 effects offers a rare opportunity to gauge the lower limits of air pollution in the study region at the current energy consumption pattern and industrial installation.

China was the earliest country that encountered the COVID-19 epidemic and implemented control measures to stop the spread of the virus. Since Wuhan lock-down on January 23, 2020, all provinces in the China mainland implemented strict measures to reduce person-to-person contacts, ranging from keeping nonessential factories and

offices closed to travel restrictions and a high level of self home-quarantine in the population. While these measures have effectively limited the spread of the virus, it has also substantially reduced anthropogenic activities and emissions. It is of great need to measure the extent of the air quality changes as the results of the reduced human activities.

Existing studies in evaluating the COVID-19's effects on air quality tend to estimate the effects by directly comparing the periods across years, or the periods before/after the lock-down in 2020, which ignored the confounding of general air quality trend and different meteorological variation. Bauwens et al. (2020) investigated the impacts on NO_2 in China and other early epicenters using satellite observations. To eliminate the interference of the lunar new year, they compared the average NO_2 between 11 February and 24 March 2020 to the same period in 2019 and found that NO_2 dropped by 40% over 16 lock-down cities in China on average. Cadotte (2020) used the differences in the average concentrations between February in 2019 and 2020 as measures of the COVID-19 effects in six international cities. Sicard et al. (2020) assessed the effect of lock-down in four European cities and Wuhan by comparing the lock-down period in 2020 to the same periods in 2017–2019. Otmani et al. (2020) studied the impact of COVID-19 lock-down on PM_{10}, SO_2, and NO_2 in Salé of Morocco by the differences between the concentrations before and during the lock-down period. Sharma et al. (2020) studied the effects of restricted emissions on air quality in India by comparing the average concentrations in 2020 with those over the same period in the previous years.

Cares have to be exercised when quantifying the COVID-19 effects on air quality. In particular, meteorological confounding has to be considered. Temperature, which is a driver for ozone, naturally increases from early January to after Wuhan lock-down on January 23, 2020. Hence, the increase in a factor of 1.5–2 found in Shi and Brasseur (2020) in the ozone was partly due to more solar radiation in the warmer COVID-19 control period. A calculation given in the supplementary materials (SM) shows that similar increases in the ozone happened over the same time periods in 2019.

Another issue is the air quality trend which prevents simple yearly matching and comparison. This is particularly needed in China as the air pollution mitigation initiatives since 2013 (State Council of China, 2013) has led to significant reductions in $PM_{2.5}$, PM_{10}, and SO_2 in North China (Chen et al., 2018; Liu et al., 2019; Shen et al., 2017; Tânia et al., 2017). At the same time, there has been an increasing trend in ozone (O_3) (Tan et al., 2018; Wang et al., 2019). Hence, a direct comparison between the COVID-19 control period in 2020 and the same time period in 2019 would mix the effects of the yearly trends and the COVID-19 lock-down measures.

There are studies on statistical models with applications to air quality. Fassó and Finazzi (2013) proposes a spatiotemporal model with time-varying coefficient and latent variables, and applications in mapping the daily average NO_2 concentration in Europe; see Wan et al. (2021) for extension to China's air pollution modeling. Liang et al. (2015) and Zhang et al. (2020) proposed a nonparametric spatial and temporal adjustment to the meteorological confounding in air quality assessments.

A key in the COVID-19 effect study is to impute the would-be average pollution concentrations in the absence of the COVID-19. We propose a Difference in Relative-Difference (DiRD) method which extends the existing Different-in-Difference method (DiD) method (Angrist & Pischke, 2008; Card & Krueger, 1994; Lechner, 2011) in two aspects. As meteorology plays significant roles in the observed pollution concentrations, we adopt the flexible nonparametric regression method to remove the meteorological confounding, which is related to the semiparametric approach in Abadie (2005) and the nonparametric estimation in Lu et al. (2019). As the yearly trend of air quality is significantly impacted by human effort, we make the conditional parallel trends assumption on relative differences instead of the absolute differences.

Our study finds striking COVID-19 effects on the six major air pollutants in 68 cities in North China. The effects were the most significant on NO_2 with 67 of the 68 cities having statistically significant reductions at 5% level, followed by $PM_{2.5}$ (60 cities) and PM_{10} (48 cities), CO and O_3 in 51 and 47 cities, and SO_2 in 40 cities, respectively. It is found that NO_2 was reduced by 39.6% compared with the non-COVID-19 baseline among the 68 cities, followed by $PM_{2.5}$ (30.9%), O_3 (16.3%), PM_{10} (14.3%), CO (13.9%), and SO_2 (10.0%). The cities located in the northwest of Henan province, east of Shandong province, and a substantial area of Hebei province had the most decrease in NO_2 and $PM_{2.5}$.

The paper is organized as follows. Section 2 introduces the study design and shows evidence of meteorological confounding. Section 3 outlines the Difference in Relative-Difference (DiRD) method with the proposed estimation procedure. Section 4 contains details on the statistical inference of the estimated treatment effect. Section 5 reports the results of COVID-19 effects and analyses.

2 | DATA AND METEOROLOGICAL CONFOUNDING

This section introduces the study region and data for the study, and demonstrate the meteorological confounding on air pollution.

2.1 | Study region and data

Our study includes all 68 prefecture-level or above cities from five provinces (Hebei, Henan, Shandong, Shanxi, and Shaanxi) and two mega cities (Beijing and Tianjin) in North China. The 68 cities constitute the focal region in China's air pollution mitigation campaign (Ministry of Ecology and Environment of China, 2018), which has endured severe air pollution, largely driven by heavy industrial productions (steel, iron, and building materials).

The data are hourly measurements of six major air pollutants: $PM_{2.5}$, PM_{10}, NO_2, SO_2, CO, and O_3 from 368 monitoring sites administrated by the China National Environmental Monitoring Centre. We consider meteorological variables from China's Central Meteorological Agency (CMA) as confounding covariates for the causal inference. The meteorological variables include air pressure (PRES), surface air temperature (TEMP), surface dew point temperature (DEWP), wind direction (cbwd), cumulative wind velocity (Iws), and cumulative precipitation (IRAIN). The wind directions are grouped into five categories: NW, NE, SW, SE and CV, where NE = {NE,NNE,ENE}, NW = {W,N,NW,NNW,WNW}, SW = {SW,SSW, WSW}, SE = {E,S,SE,ESE,SSE} and CV means calm or when the wind speed is less than 0.5 m/s. The cumulative wind speed (Iws) is the cumulation of the hourly wind speed under a wind direction and is reset to zero when the direction is changed. Similarly, the cumulative precipitation sums over the precipitation (IRAIN) since it begins to rain and is reset to zero when it stops. Each air-quality site is matched to the nearest CMA site. Figure 1 shows the geographical locations of the cities, and the air quality and meteorological sites.

Our analysis also considers monthly coal consumption and industrial outputs in the last two winters. The provincial coal consumption data were acquired from China Coal Resource Association (http://www.sxcoal.com/). The monthly major industrial outputs for iron, steel, cement, and electricity are from the National Bureau of Statistics of China. Electricity generation and metallurgy are the two largest coal consuming sectors in North China. The analysis of the coal consumption and industrial outputs are provided in the supplementary file.

2.2 | Meteorological confounding

Conventional air quality assessment is based on raw average concentrations. However, the observed concentration is subject to meteorological confounding, that makes the raw statistical measures incomparable, since the weather condition endures much variation in different years; see Liang et al. (2015) for an adjustment approach to remove the confounding.

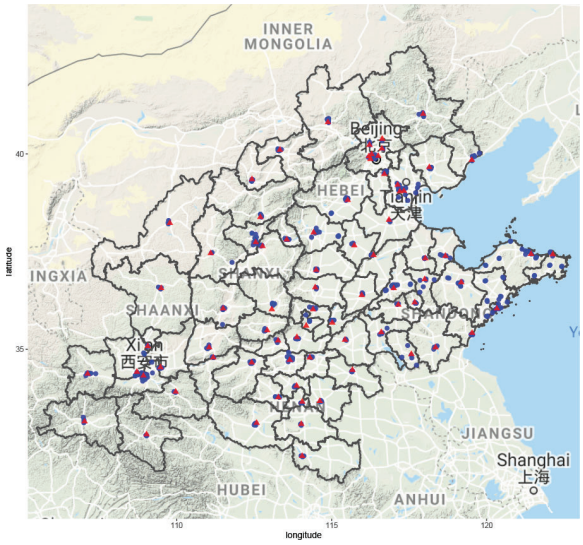

FIGURE 1 The study region consisting of 68 cities from the five provinces plus Beijing and Tianjin in North China with locations of air-quality monitoring stations in blue bullets and the meteorological stations in red triangles

Figure 2 displays the scatter plots of two meteorological variables (the dew point and pressure) at two sites (Beichen in Tianjin and Linfen Gongshan in Shanxi) during four periods in January, February in 2019 and 2020, respectively. The panel of February in 2020 largely corresponds to the COVID-19 control period. $PM_{2.5}$ concentration is signified by color. It is shown from the panels that higher $PM_{2.5}$ is associated with higher dew point when the meteorological condition is favorable for secondary generation of $PM_{2.5}$. The confounding effect of the air pressure is less pronounced than that of the dew point. Figure 2 also reveals varying distributions of meteorological conditions between the 2 years, shown by the marginal density plots on the top and right edges of the panels. Compared with February 2019, the distribution of the dew point in February 2020 is more skewed with higher values for both sites. This implies that the meteorological condition in 2020 is less favorable than the same period in 2019, and hence we should not directly compare the raw $PM_{2.5}$ averages over the two periods when estimating the COVID-19 effects. Further, the panel of the lock-down period in February 2020 shows a visible reduction in the $PM_{2.5}$ relative to the other panels, which suggests that the lock-down did mitigate the pollution of $PM_{2.5}$ even under an unfavorable meteorological condition.

3 | STUDY DESIGN AND MODELING

In this section, we present the proposed Difference in Relative-Difference (DiRD) method for estimating the COVID-19 effect by introducing the study design, the nonparametric regression and the estimation for the treatment effect.

3.1 | Study design

A direct comparison of pollution concentrations between the COVID-19 control period in 2020 and the corresponding period in 2019 would mix the COVID-19 effects with nonrelated mitigation measures. A valid approach is to compare the observed concentrations over the COVID-19 control period with the counterfactual concentrations in the absence of the lock-down in the same COVID-19 period in 2020 after adjusting for the meteorological confounding.

The DiRD method uses a design of four study periods shown in Table 1. The period before the lock-down is from December 1, 2019 to January 22, 2020, while the lock-down period is from January 31 to February 29 in 2020. There is an 8-day gap between the two periods to avoid the lunar new year (LNY) holidays effect, because the LNY day is the most important holiday in China during which nonessential industrial and service operations are suppressed and also alters the general emission and air quality profiles. Similarly, two matching periods in the previous year were defined, where the 8-day LNY gap was determined according to the LNY day in 2019.

3.2 | Regression on meteorological data

Let Y_{ijt} be the concentration of a pollutant and $\boldsymbol{X}_{ijt} = (\boldsymbol{Z}'_{ijt}, W_{ijt})'$ be the meteorological variables at time t of winter season i ($i = 2019$ for the 2018–2019 winter and $i = 2020$ for the 2019–2020 winter seasons, respectively) and a study period j ($j = 1$ before and $j = 2$ after the LNY) in a monitoring site of a city, where $\boldsymbol{Z}_{ijt}$ is a vector of continuous meteorological variables and W_{ijt} is the discrete wind direction.

As the concentrations of air pollutants are highly nonlinear with respect to meteorological variables, we do not impose parametric specifications on the regression functions and let the data decide the form instead. For each period, we study the meteorological impacts on Y_{ijt} of a pollutant by a nonparametric regression model (Härdle, 1990):

$$Y_{ijt} = m_{ij}(\boldsymbol{X}_{ijt}(s)) + \sigma_{ij}\left(\mathbf{X}_{ijt}(s)\right) e_{ijt}(s), \tag{1}$$

where $m_{ij}(\boldsymbol{x}) = \mathbb{E}\{Y_{ijt}|\boldsymbol{X}_{ijt}(s) = \boldsymbol{x}\}$, $\sigma^2_{ij}(\boldsymbol{x}) = \mathrm{Var}\{Y_{ijt}|\mathbf{X}_{ijt}(s) = \boldsymbol{x}\}$ and $e_{ijt}(s)$ are the standardized residuals satisfying that $\mathbb{E}\{e_{ijt}(s)|\boldsymbol{X}_{ijt}(s)\} = 0$ and $\mathrm{Var}\{e_{ijt}(s)|\boldsymbol{X}_{ijt}(s)\} = 1$. The residuals $\{e_{ijt}(s)\}$ are spatially and temporally stationary and satisfy the α-mixing conditions as in Zhang et al. (2020).

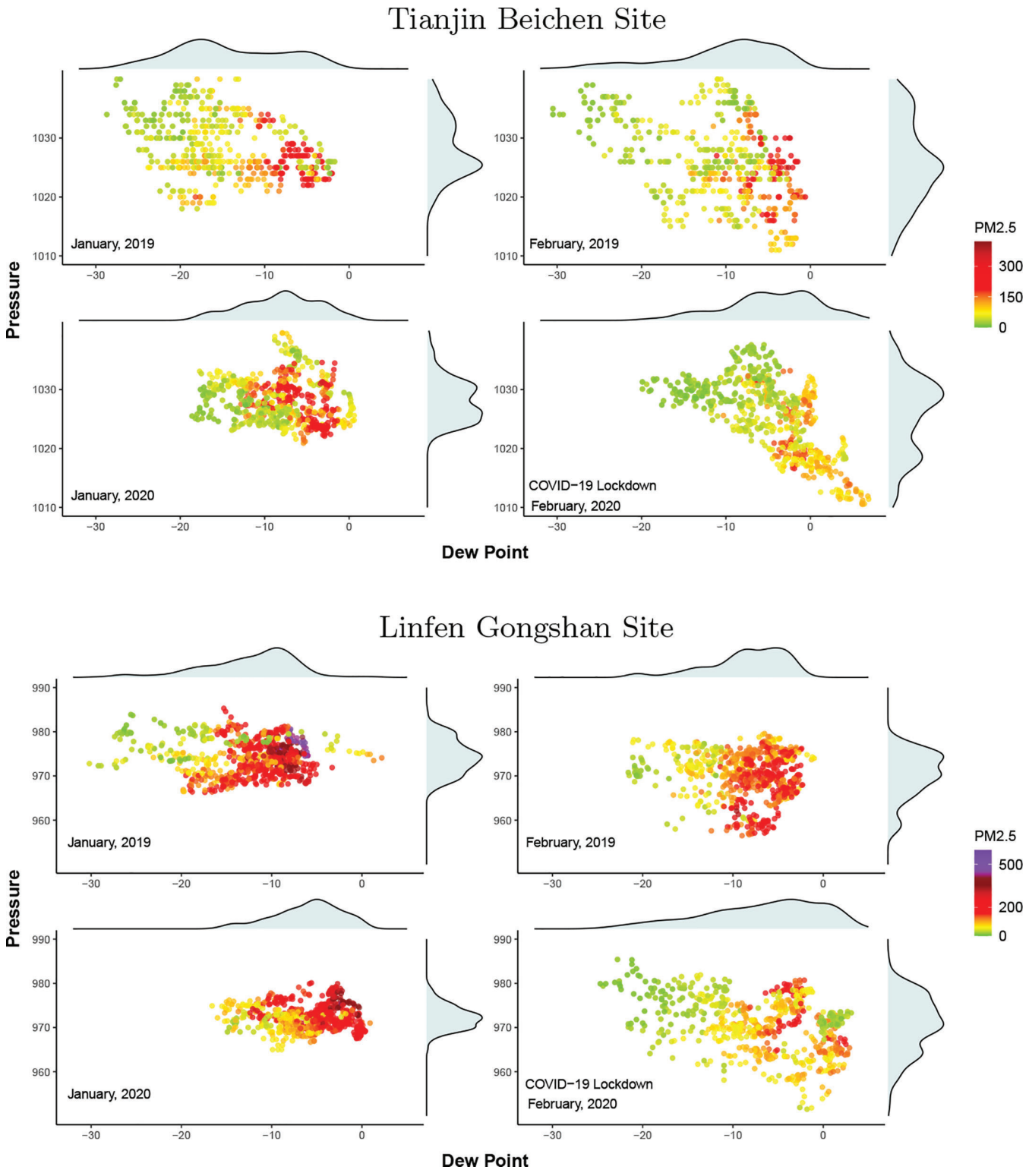

FIGURE 2 Scatter plots of the dew point temperature (DEWP) and the air pressure (PRES) with $PM_{2.5}$ level superimposed by color in January and February in 2019 and 2020, respectively. The marginal densities of Dew Point and Pressure are shown on the upper and right edges

Dec-01-2018 to Feb-02-2019	8-day gap of LNY	Feb-11-2019 to Feb-28-2019
2019, Period 1		2019, Period 2
Dec-01-2019 to Jan-22-2020	8-day gap of LNY	**Jan-31-2020 to Feb-29-2020**
2020, Period 1		**2020, Period 2**

TABLE 1 The four periods in the Difference in Relative-Difference study design, with 8-day gaps that correspond to the lunar new year (LNY) holidays

Note: The bold text represents the COVID-19 period in the study.

We consider the Nadaraya–Watson (NW) kernel smoothing estimator to estimate $m(\boldsymbol{x})$. Suppose that for the period (i,j), we have n_{ij} hourly observations $\{(\boldsymbol{X}_{ijt}, Y_{ijt})\}_{t=1}^{n_{ij}}$ from a monitoring site. The NW estimator of $m_{ij}(\boldsymbol{x})$ is

$$\hat{m}_{ij}(\boldsymbol{x}) = \frac{\sum_{t=1}^{n_{ij}} K_{\boldsymbol{H}}\left(\boldsymbol{z} - \boldsymbol{Z}_{ijt}\right) Y_{ijt} I\left(W_{ijt} = w\right)}{\sum_{t=1}^{n_{ij}} K_{\boldsymbol{H}}\left(\boldsymbol{z} - \boldsymbol{Z}_{ijt}\right) I\left(W_{ijt} = w\right)}, \tag{2}$$

where $K_{\boldsymbol{H}}(\boldsymbol{z}) = (k(z_1/h_1) \ \dots \ k(z_d/h_d)) / (h_1 \ \dots \ h_d)$ is a product kernel generated by the univariate kernel function $k(\cdot)$ for $\boldsymbol{x} = (\boldsymbol{z}', w)', \boldsymbol{z} = (z_1, \ \dots \ , z_d)'$ and smoothing bandwidths $\boldsymbol{H} = (h_1, \ \dots \ , h_d)'$, and $I\left(W_{ijt} = w\right)$ is the indicator function for a wind direction w. In implementation, we use the Gaussian kernel $k(u) = (2\pi)^{-1/2} \exp(-u^2/2)$ and the cross-validation (CV) method to select the smoothing bandwidths $\boldsymbol{H}$ (Härdle, 1990).

There are two issues that require discussion. One is that the product kernel is a common way to do multivariate smoothing without implying different dimensions of the data being independent, as shown theoretically in Simonoff (2012). Another issue is that the spatial and temporal dependence in the residuals would not affect the estimation consistency as shown in Zhang et al. (2020), although they would affect the efficiency and the variance estimation. This is the reason for employing the spatial–temporal bootstrap in estimating the standard errors in Section 4.

3.3 | Difference in relative-difference method

For simplicity, we omit the time index t from now on and use Y_{ij} and $\boldsymbol{X}_{ij}$ as generic notations for pollutant concentrations and the meteorological conditions in winter season i and period j. We adopt the notion of potential outcomes (Rubin, 1974) to define the COVID-19 control effects on air quality.

Let $Y_{ij}(0)$ be the potential outcome that would be observed in the absence of lock-down treatment for the year i (2019 or 2020) and a study period j (1 before and 2 after the LNY) and $Y_{ij}(1)$ be the counterpart that would be observed under the lock-down treatment. Only one of the two potential outcomes can be observed for each period. For the three periods $(i,j) = (2019,1), (2019,2)$, and $(2020,1)$, $Y_{ij} = Y_{ij}(0)$ as there was no lock-down treatment, and $Y_{2020,2} = Y_{2020,2}(1)$ corresponds to the COVID-19 lock-down period.

We define the average treatment effect with the meteorological adjustment:

$$\tau = \mathbb{E}_{\boldsymbol{X}}\left[\mathbb{E}\left(Y_{2020,2}(1) - Y_{2020,2}(0) | \boldsymbol{X}_{2020,2} = \boldsymbol{x}\right)\right] = \int \tau(\boldsymbol{x}) dF_{\mathbf{X}}(\boldsymbol{x}), \tag{3}$$

where $\tau(\boldsymbol{x}) = \mathbb{E}\left(Y_{2020,2}(1) - Y_{2020,2}(0) | \boldsymbol{X}_{2020,2} = \boldsymbol{x}\right)$ is the conditional average treatment effect, and $F_{\mathbf{X}}$ is the baseline meteorological distribution in the long run and estimated using the meteorological data of Februaries since 2011. Let $m^0_{2020,2}(\boldsymbol{x}) = E(Y_{2020,2}(0) | \boldsymbol{X}_{2020,2} = \boldsymbol{x})$ denote the would-be conditional average at a $\boldsymbol{x}$. Hence, $\tau(\boldsymbol{x}) = m_{2020,2}(\boldsymbol{x}) - m^0_{2020,2}(\boldsymbol{x})$. As $m_{2020,2}(\boldsymbol{x})$ can be estimated by (2), the key is to estimate $m^0_{2020,2}(\boldsymbol{x})$. Let $\mu(1) = \int m_{2020,2}(\boldsymbol{x}) dF_{\mathbf{X}}(\boldsymbol{x})$ and $\mu(0) = \int m^0_{2020,2}(\boldsymbol{x}) dF_{\mathbf{X}}(\boldsymbol{x})$ be the meteorologically adjusted means of the potential outcomes $Y_{2020,2}(1)$ and $Y_{2020,2}(0)$, respectively. Then, $\tau = \mu(1) - \mu(0)$. We use $\tau/\mu(0)$ to compare the relative effects between different pollutants and regions.

The conventional Difference-in-Difference (DiD) estimator requires the global parallel-trend assumption $\mathbb{E}[Y_{2020,2}(0) - Y_{2020,1}(0)] = \mathbb{E}[Y_{2019,2}(0) - Y_{2019,1}(0)]$, which means that the difference of the average outcomes of the treated and control periods is invariant in the absence of the policy intervention, and leads to the average treatment effect $\mathrm{E}[Y_{2020,2}(1) - Y_{2020,2}(0)] = \mathbb{E}(Y_{2020,2} - Y_{2020,1}) - \mathbb{E}(Y_{2019,2} - Y_{2019,1})$. However, such assumption is unreasonable in

our study for two reasons. First, it is implausible to assume that the absolute decrease across periods from $j=1$ to $j=2$ would be the same in the two years when the initial levels in the period 1 of the 2 years are quite different. Take the city of Linfen as an example. Its SO_2 average was 94 μg/m^3 in period 1 and 53 μg/m^3 in period 2 of 2019. It is hard to argue that such the difference 41 μg/m^3 happened in 2019 is maintained in 2020 as the first period concentration in 2020 was 48 μg/m^3. Another reason is that air pollution is much affected by meteorological conditions, and the meteorological distribution may not be the same in different periods.

We assume a relative conditional parallel-trend condition formulated as

$$\frac{m^0_{2020,2}(\boldsymbol{x}) - m_{2020,1}(\boldsymbol{x})}{m_{2020,1}(\boldsymbol{x})} = \frac{m_{2019,2}(\boldsymbol{x}) - m_{2019,1}(\boldsymbol{x})}{m_{2019,1}(\boldsymbol{x})}. \tag{4}$$

Note that $m^0_{2020,2}(\boldsymbol{x})$ is the regression function of $Y_{2020,0}(0)$, which is unobservable. Although (4) cannot be fully verified, we can check it using past years' data not affected by the epidemic. We consider 2017 and 2019 with the corresponding two periods before and after the LNY. We select 2017 because the solar calendar date of LNY in 2017 was closer to 2019 than that of 2018. The DiRD assumption on 2017 and 2019 can be written as $\frac{m_{2019,2}(\boldsymbol{x})-m_{2019,1}(\boldsymbol{x})}{m_{2019,1}(\boldsymbol{x})} = \frac{m_{2017,2}(\boldsymbol{x})-m_{2017,1}(\boldsymbol{x})}{m_{2017,1}(\boldsymbol{x})}$, which is equivalent to $\Delta(\boldsymbol{x}) =: \frac{m_{2019,2}(\boldsymbol{x})}{m_{2019,1}(\boldsymbol{x})} - \frac{m_{2017,2}(\boldsymbol{x})}{m_{2017,1}(\boldsymbol{x})} = 0$.

To verify the assumption, we compute the estimates $\hat{\Delta}(\boldsymbol{x}_i)$ by using the NW estimate $\hat{m}_{i,j}(\boldsymbol{x})$ at the meteorological observations $\{\boldsymbol{x}_i\}_{i=1}^N$ in all Februaries of the last 10 years. Figure 3 displays the estimated $\hat{\Delta}(\boldsymbol{x}_i)$ with $PM_{2.5}$ and NO_2 as the outcome variable. The figure provides the density plots of $\hat{\Delta}(\boldsymbol{x}_i)$ and the scatter plots for the four meteorological variables: DEWP (dew point), Iws (cumulative wind speed), PRES (pressure), and TEMP (temperature). The figures for PM_{10}, SO_2, CO, and O_3 are included in the supplementary. The figure shows $\hat{\Delta}(\boldsymbol{x}_i)$ was largely distributed around zero and lends support to the assumption of $\Delta(\boldsymbol{x}) = 0$.

Based on the assumption (4), the unobserved would-be regression function

$$m^0_{2020,2}(\boldsymbol{x}) = m_{2020,1}(\boldsymbol{x}) + \frac{m_{2020,1}(\boldsymbol{x})}{m_{2019,1}(\boldsymbol{x})}\{m_{2019,2}(\boldsymbol{x}) - m_{2019,1}(\boldsymbol{x})\} \tag{5}$$

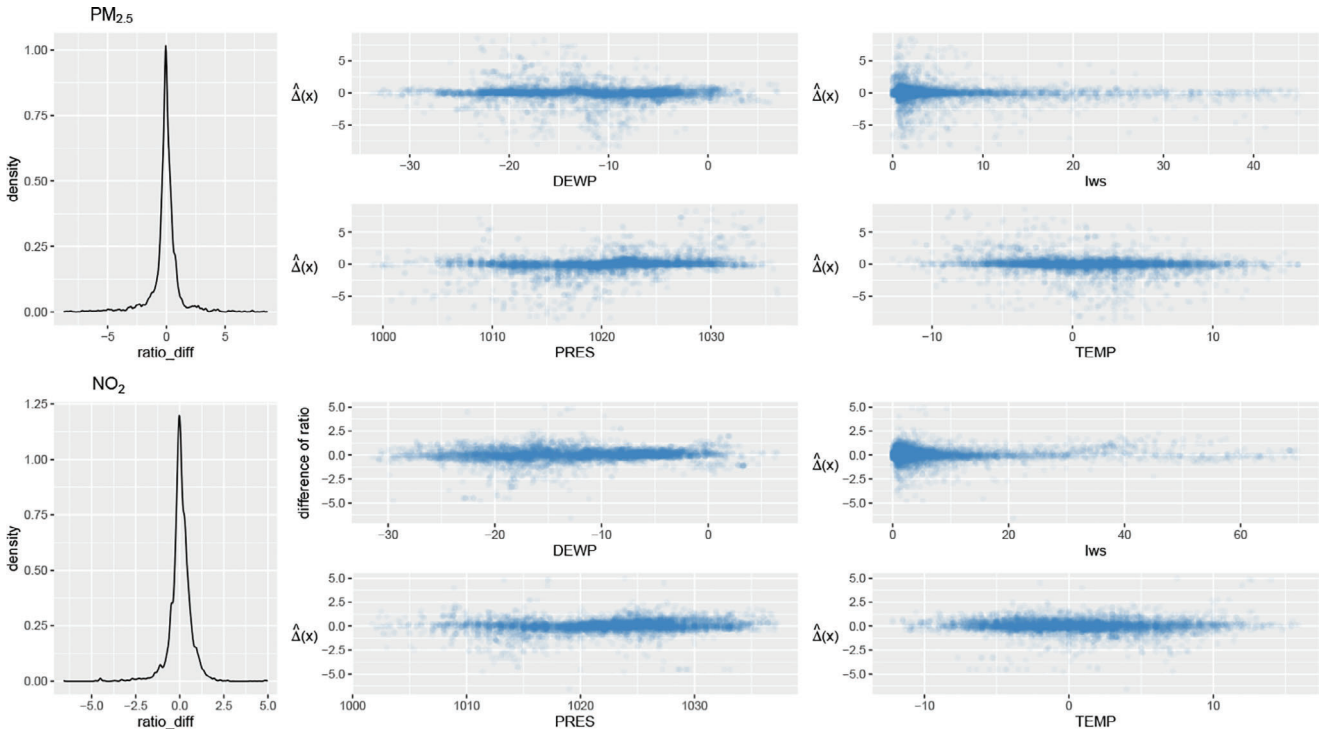

FIGURE 3 The distribution of $\hat{\Delta}(\boldsymbol{x}_i)$ for $PM_{2.5}$ and NO_2, respectively. In each figure, the left panel is the density plots of $\hat{\Delta}(\boldsymbol{x}_i)$, and the four panels on the right are the scatter plots between $\hat{\Delta}(\boldsymbol{x}_i)$ and the meteorological variables

and thus

$$\tau(\boldsymbol{x}) = \{m_{2020,2}(\boldsymbol{x}) - m_{2020,1}(\boldsymbol{x})\} - \frac{m_{2020,1}(\boldsymbol{x})}{m_{2019,1}(\boldsymbol{x})}\{m_{2019,2}(\boldsymbol{x}) - m_{2019,1}(\boldsymbol{x})\}. \tag{6}$$

By estimating each $m_{ij}(\boldsymbol{x})$ using the NW estimator, we attain the estimator $\hat{\tau}(\boldsymbol{x})$ and the COVID-19 effects by averaging $\hat{\tau}(\boldsymbol{x})$ over all February's meteorological data from 2011 to 2020, say $\{\boldsymbol{X}_t\}_{t=1}^{T}$, namely

$$\hat{\tau} = \frac{1}{T}\sum_{t=1}^{T}\hat{\tau}(\boldsymbol{X}_t). \tag{7}$$

Similarly, we have $\hat{\mu}(1) = \frac{1}{T}\sum_{t=1}^{T}\hat{m}_{2020,2}(\mathbf{X}_t)$ and $\hat{\mu}(0) = \frac{1}{T}\sum_{t=1}^{T}\hat{m}^0_{2020,2}(\mathbf{X}_t)$. The estimation procedure is conducted for each air quality monitoring site with the meteorological data from the matched weather site. The citywise COVID-19 effect is estimated by averaging over all monitoring sites in a city.

One may need to demonstrate the relationship between the pollutant's concentration and a univariate meteorological variable. We define the marginal dependence function with respect to one variable $X^{(k)}$ while removing the confounding of the other variables denoted as $\mathbf{X}^{(-k)}$. Let $g(\boldsymbol{x}) = g(x^{(k)}, \boldsymbol{x}^{(-k)})$ be a generic multivariate function of $\boldsymbol{x}$, and

$$g^{(k)}(x^{(k)}) = \int g(x^{(k)},\ \boldsymbol{x}^{(-k)})dF_{\boldsymbol{X}^{(-k)}|x^{(k)}}(\boldsymbol{x}^{(-k)}) \tag{8}$$

be the marginal dependence function, where $F_{\boldsymbol{X}^{(-k)}|x^{(k)}}$ is the conditional distribution of $\mathbf{X}^{(-k)}$ on $X^{(k)} = x^{(k)}$ derived from the baseline meteorological distribution $F_{\mathbf{X}}$. By substituting $g(\boldsymbol{x})$ with the conditional effect $\tau(\boldsymbol{x})$, the regression function $m_{2020,2}(\boldsymbol{x})$, and the counterfactual regression function $m^0_{2020,2}(\boldsymbol{x})$, we obtain the univariate functions $\tau^{(k)}(\cdot)$, $m^{(k)}_{2020,2}(\cdot)$, and $m^{0(k)}_{2020,2}(\cdot)$.

For estimation, by the law of large numbers, we may use the baseline meteorological data $\{\mathbf{X}_t\}_{t=1}^{T}$ over the 10 years to estimate (8) by $\hat{g}^{(k)}(x^{(k)}) = \frac{\sum_{\mathbf{X}_t \in A(x^{(k)},b)}\hat{g}(\mathbf{X}_t)}{N(x^{(k)},b)}$, where $A(x^{(k)}, b) = \{\mathbf{X}_t : |X_t^{(k)} - x^{(k)}| \le b\}$ is the cross-section of the X-domain which has its component $X_t^{(k)}$ within a neighborhood of $x^{(k)}$, $N(x^{(k)}, b)$ is sample size within $A(x^{(k)}, b)$, b is a smoothing parameter.

Figure 4 displays the estimated marginal dependence function $\hat{m}^{(k)}_{2020,2}(x^{(k)})$, the counterfactual one $\hat{m}^{0(k)}_{2020,2}(x^{(k)})$, and the marginal treatment effect $\hat{\tau}^{(k)}(x^{(k)})$ with $x^{(k)}$ being the dew point and temperature, respectively. As shown in these functions, the concentration of air pollutants tends to increase when the dew point increases, while the confounding effect of the temperature is less pronounced. Besides, the estimated counterfactual curves $\hat{m}^{0(k)}_{2020,2}(x^{(k)})$ were higher than the observed $\hat{m}^{(k)}_{2020,2}(x^{(k)})$, which was an early sign for the COVID-19 control measures' effect on reducing the potential level of air pollution consistently over the dew point and the temperature variables, respectively.

4 | INFERENCE FOR THE TREATMENT EFFECT

In this section, we consider statistical inference for $\hat{\tau}$ and in particularly the variance estimation. The spatial–temporal dependence in the residuals of Model (1) has to be considered. Note that $\hat{\tau} - \tau$ admits an expansion after some algebraic manipulations:

$$\hat{\tau} - \tau = I_1 + I_2 + o_p(n_{ij}^{-\frac{1}{2}}), \tag{9}$$

where $I_1 = \int (\hat{\tau}(\boldsymbol{x}) - \tau(\boldsymbol{x}))\, dF_{\mathbf{X}}(\boldsymbol{x})$ and

$$I_2 = \int \tau(\boldsymbol{x})d\{\hat{F}_{\boldsymbol{X}}(\boldsymbol{x}) - F_{\boldsymbol{X}}(\boldsymbol{x})\} = \sum_{i=2011}^{2020}\left[(T)^{-1}\sum_{t=1}^{n_{i2}}\tau(\boldsymbol{X}_{i2t}) - \frac{1}{10}\int \tau(\boldsymbol{x})dF_{\boldsymbol{X}_{i2}}(\boldsymbol{x})\right].$$

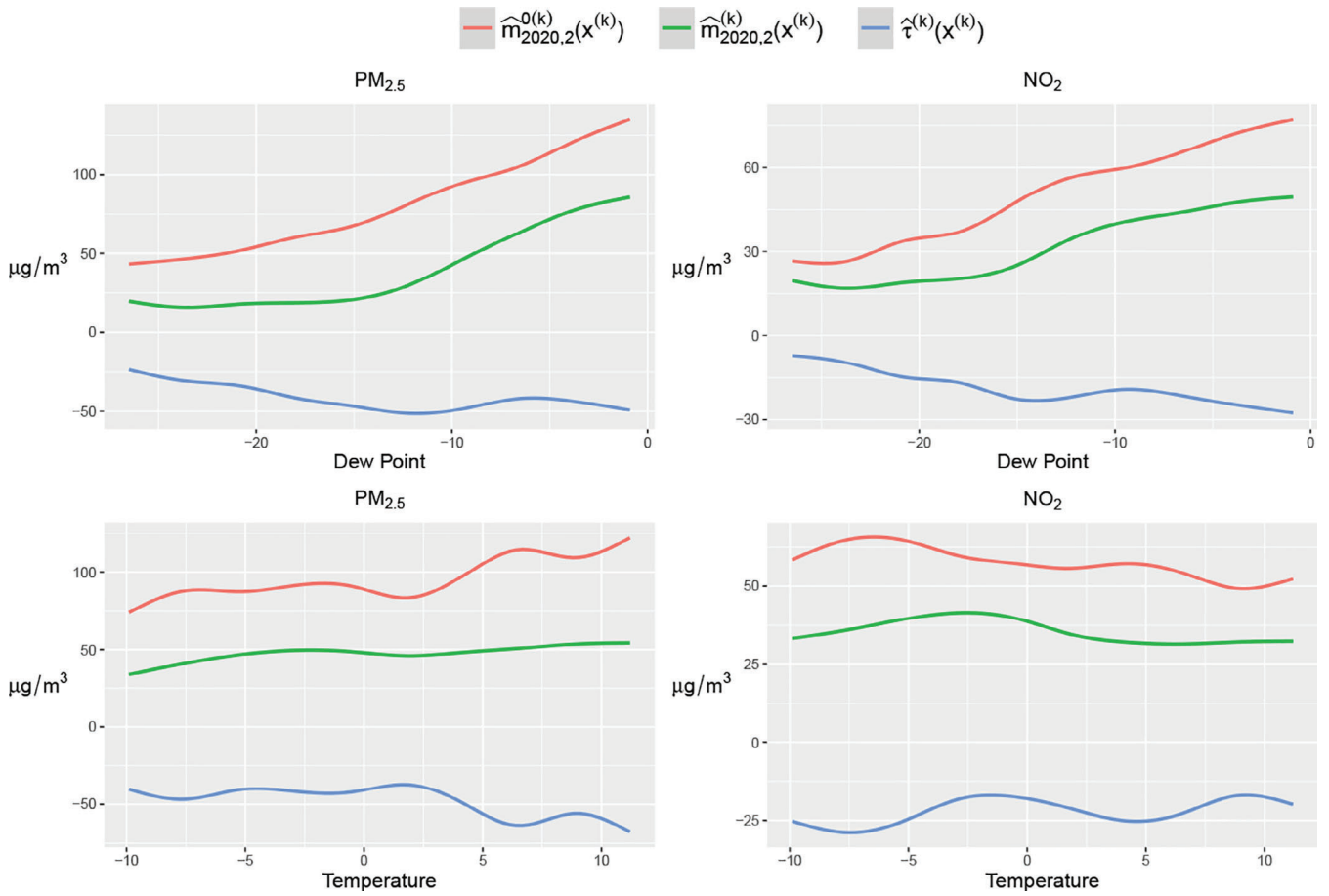

FIGURE 4 Estimated marginal dependence functions $\hat{m}^{(k)}_{2020,2}(x^{(k)})$, the counterfactual regression function $\hat{m}^{0(k)}_{2020,2}(x^{(k)})$, and the conditional treatment effect $\hat{\tau}^{(k)}(x^{(k)})$ with $X^{(k)}$ being the dew point and temperature for $PM_{2.5}$ and NO_2 using data from Tianjin Beichen site. The smoothing bandwidth $b = 2.8$ for the dew point and $b = 2.1$ for the temperature

These two terms are resulted from the estimation errors in the regression function and the baseline meteorological distributions, respectively. It may be shown, by following the approach in Zhang et al. (2020) (section 4), that $\hat{\tau}$ is asymptotically normally distributed with τ being the asymptotic mean under certain conditions. The asymptotic variance of $\hat{\tau}$ is very involved as both the spatial and temporal dependence get involved in the variance expression.

To facilitate statistical inference, we propose a spatiotemporal block bootstrap method to approximate the null distribution of $\hat{\tau}$. The bootstrap strategy combines the temporal block bootstrap on the meteorological variables with the wild bootstrap that resamples the residuals of the regression model. The bootstrap simulates the distribution of $\hat{\tau}$ under the null hypothesis of no COVID-19 effects, which gives the p-values for testing $H_0 : \tau = 0$ versus $H_1 : \tau < 0$.

To implement the bootstrap, we need to estimate the conditional variance $\sigma^2_{ij}(\boldsymbol{x})$ of the residuals ε_{ijt}, which is conducted by the kernel smoothing method on $\hat{\varepsilon}^2_{ijt} = \{Y_{ijt} - \hat{m}_{ij}(\boldsymbol{X}_{ijt})\}^2$, so that for $\boldsymbol{x} = (\boldsymbol{z}', w)'$

$$\hat{\sigma}^2_{ij}(\boldsymbol{x}) = \frac{\sum_{t=1}^{n_{ij}} K_{\tilde{\boldsymbol{H}}}\{\boldsymbol{z} - \boldsymbol{Z}_{ijt}\}\hat{\varepsilon}^2_{ijt} I\{W_{ijt} = w\}}{\sum_{t=1}^{n_{ij}} K_{\tilde{\boldsymbol{H}}}\{\boldsymbol{z} - \boldsymbol{Z}_{ijt}\} I\{W_{ijt} = w\}}. \tag{10}$$

The bandwidths vector $\tilde{\boldsymbol{H}}$ is selected by the CV (Härdle, 1990). These lead to the estimated standardized residuals $\hat{e}_{ijt} = \hat{\varepsilon}_{ijt}/\hat{\sigma}_{ij}(\boldsymbol{X}_{ijt})$. As shown in Figure 1, the air-quality monitoring sites in different cities are well separated from each other with at least 50 km apart from each other, which would imply a weak spatial dependence among $\{\hat{e}_{ijt}\}$ between sites in different cities. As shown by the semi-varigrams in Figures 2 and S1 of Zhang et al. (2020), there were little spatial dependence beyond 20 km among the residuals. Hence, we conducted citywise bootstrap resampling of the residuals

with respect to the spatial scale. Specifically, suppose there are R air-quality monitoring sites in a city, which are denoted as $s_1, \dots, s_R$. Let $\hat{\mathbf{E}}_{ijt} = \{\hat{e}_{ijt}(s_1), \dots, \hat{e}_{ijt}(s_R)\}'$ and

$$\hat{\Sigma}_{ij} = n_{ij}^{-1} \sum_{t=1}^{n_{ij}} \hat{\mathbf{E}}_{ijt} \hat{\mathbf{E}}_{ijt}^{'} - \left(n_{ij}^{-1} \sum_{t=1}^{n_{ij}} \hat{\mathbf{E}}_{ijt} \right) \left(n_{ij}^{-1} \sum_{t=1}^{n_{ij}} \hat{\mathbf{E}}_{ijt}^{'} \right).$$

Both $\hat{\sigma}_{ij}^2(\boldsymbol{x})$ and $\hat{\Sigma}_{ij}$ are used for resampling the residuals later.

Then, we construct the bootstrapped samples of covariates and responses for each period (i, j) except the period $i = 2020, j = 2$, which was under COVID-19 control. We combine the meteorological data used for the air-quality monitoring stations in a city to form the time series $\boldsymbol{X}_t = \{\boldsymbol{X}'_{ijt}(s_1), \dots, \boldsymbol{X}'_{ijt}(s_R)\}'$, $t = 1, \dots, n_{ij}$. Consider moving blocks with length l: $B_1 = (\boldsymbol{X}_1, \dots, \boldsymbol{X}_l), \dots, B_{n_{ij}-l+1} = (\boldsymbol{X}_{n_{ij}-l+1}, \dots, \boldsymbol{X}_{n_{ij}})$, $B_{n_{ij}-l+2} = (\boldsymbol{X}_{n_{ij}-l+2}, \dots, \boldsymbol{X}_{n_{ij}}, \boldsymbol{X}_1), \dots, B_{n_{ij}} = (\boldsymbol{X}_{n_{ij}}, \boldsymbol{X}_1, \dots, \boldsymbol{X}_{l-1})$. Similar to Liang et al. (2015) and Zhang et al. (2020), we set $l = 12$ h. The wrapping at the boundary ensures that each of the original observations appears with an equal chance in a bootstrapped sample. Then n_{ij}/l blocks are randomly selected from the total of n_{ij} blocks with replacement, which are joined together to form the resampled meteorological time series $\{\boldsymbol{X}^*_{ijt}(s)\}_{t=1}^{n_{ij}}$.

Based on $\{\boldsymbol{X}^{*b}_{ijt}(s)\}_{t=1}^{n_{ij}}$, the resampled covariates from the bth round of resampling at site s among $s_1, \dots, s_R$, we impute the times series of outcome variable via the estimated regression function $\hat{m}_{ij}$ and resampled residuals $\hat{\varepsilon}^{*b}_{ijt}(s)$ by

$$Y^{*b}_{ijt}(s) = \hat{m}_{ij}(\boldsymbol{X}^{*b}_{ijt}(s)) + \hat{\varepsilon}^{*b}_{ijt}(s), \tag{11}$$

where $\hat{\varepsilon}^{*b}_{ijt}(s) = \hat{\sigma}_{ij}(\boldsymbol{X}^{*b}_{ijt}(s))\hat{e}^{*b}_{ijt}(s)$ and $\hat{\mathbf{E}}^{*b}_{ijt} = \{\hat{e}^{*b}_{ijt}(s_1), \dots, \hat{e}^{*b}_{ijt}(s_R)\}' \sim N_R(0, \hat{\Sigma}_{ij})$.

For simplicity of the notation, we omit s in the covariates and response. By using the bth resampled data $\{\boldsymbol{X}^{*b}_{ijt}, Y^{*b}_{ijt}\}_{t=1}^{n_{ij}}$, we refit the model and calculate the regression function to generate the counterfactual

$$m^{0*b}_{2020,2}(\boldsymbol{x}) = \hat{m}^{*b}_{2020,1}(\boldsymbol{x}) + \frac{\hat{m}^{*b}_{2020,1}(\boldsymbol{x})}{\hat{m}^{*b}_{2019,1}(\boldsymbol{x})} (\hat{m}^{*b}_{2019,2}(\boldsymbol{x}) - \hat{m}^{*b}_{2019,1}(\boldsymbol{x})),$$

which leads to $\hat{\tau}^{*b}$, the bth resample of $\hat{\tau}$. Let $\{\boldsymbol{X}_t\}_{t=1}^{T}$ be the meteorological baseline (all the February meteorological data from 2011 to 2020). A similar block bootstrap can be applied to $\{\boldsymbol{X}_t\}_{t=1}^{T}$ to form the bootstrapped meteorological baseline $\{\boldsymbol{X}^{*b}_t\}_{t=1}^{T}$. To respect the null hypothesis $\tau = 0$, that is, no COVID-19 lock-down effects, the bootstrapped counterfactual data $Y(0)$ for no COVID-19 period (period 2 in 2020) is obtained via

$$Y^{*b}_{2020,2,t}(0) = m^{0*b}_{2020,2}(\boldsymbol{X}^{*b}_t) + \hat{\varepsilon}^{*b}_{2020,2,t},$$

where $\hat{\varepsilon}^{*b}_{2020,2,t}$ is generated the same way as the residuals in (11). Based on the counterfactual data $\{\boldsymbol{X}^{*b}_t, Y^{*b}_{2020,2,t}(0)\}_{t=1}^{T}$, we obtain the estimated regression function $\hat{m}^{0*b}_{2020,2}(\cdot)$ by the kernel smoothing and the average treatment effect

$$\hat{\tau}^{*b} = \frac{1}{T} \sum_{t=1}^{T} \left[\hat{m}^{0*b}_{2020,2}(\boldsymbol{X}^{*b}_t) - m^{0*b}_{2020,2}(\boldsymbol{X}^{*b}_t) \right].$$

With a total number of $B = 300$ replications, we obtain the bootstrap estimate of the null distribution of $\hat{\tau}$ via the empirical distribution of $\{\hat{\tau}^{*b}\}_{b=1}^{B}$ and calculate the p-value as $\sum_{b=1}^{B} I(\hat{\tau}^{*b} < \hat{\tau})/B$. We reject the null hypothesis if the p-value is smaller than a significant level.

5 | RESULTS AND DISCUSSION

We report results on the COVID-19 effects on the air quality using the proposed $\hat{\tau}$, and compare with the simple methods without undergoing the causal inference and meteorological adjustment by directly comparing raw averages.

TABLE 2 The COVID-19 lock-down effects $\hat{\tau}$, with the associated levels of statistical significance and 90% confidence intervals on $PM_{2.5}$ ($\mu g/m^3$), PM_{10} ($\mu g/m^3$), NO_2 ($\mu g/m^3$), CO (mg/m^3), SO_2 ($\mu g/m^3$), O_3 ($\mu g/m^3$) over the treatment period January 31 to February 29, 2020, where ***, **, *, and . mean the effect is significant less than 0 at levels .001, .01, .05, and .1, respectively. (Part of the cities are shown, the complete version is in the SM)

City	$PM_{2.5}$	PM_{10}	NO_2	SO_2	O_3	CO
Beijing	-22.24^{***}	-8.7^{***}	-12.88^{***}	-3.68^{**}	-30.38^{***}	-0.14^{***}
	(−25.97, −18.51)	(−9.91, −7.5)	(−14.04, −11.72)	(−5.04, −2.31)	(−36.81, −23.95)	(−0.15, −0.12)
Tianjin	-44.28^{***}	-31.93^{***}	-29.88^{***}	-1.3^{**}	4.13	-0.58^{***}
	(−47.06, −41.49)	(−33.22, −30.64)	(−30.56, −29.19)	(−2.14, −0.45)	(−0.7, 8.96)	(−0.61, −0.55)
Baoding	-12.74^{***}	-11.96^{***}	-21.11^{***}	-1.76^{***}	-17.04^{***}	-0.08^{***}
	(−13.93, −11.54)	(−12.95, −10.98)	(−21.56, −20.66)	(−1.93, −1.59)	(−18.87, −15.2)	(−0.09, −0.07)
Cangzhou	-19.3^{***}	-19.87^{***}	-17.2^{***}	1.15	1.4	-0.39^{***}
	(−20.38, −18.22)	(−20.88, −18.85)	(−17.59, −16.81)	(0.98, 1.33)	(0.18, 2.62)	(−0.4, −0.37)
Chengde	2.28	4.14	-10.84^{***}	0.43	-22.48^{***}	0.01
	(1.82, 2.75)	(3.57, 4.71)	(−11.33, −10.35)	(0.16, 0.71)	(−23.69, −21.28)	(0, 0.02)
Handan	-42.57^{***}	-36.48^{***}	-18.98^{***}	-5.02^{***}	-27.77^{***}	-0.2^{***}
	(−44.05, −41.1)	(−37.58, −35.38)	(−19.48, −18.48)	(−5.22, −4.83)	(−30.17, −25.36)	(−0.22, −0.19)
Hengshui	-38.98^{***}	-37.64^{***}	-22.42^{***}	-1.94^{***}	-5.89^{***}	-0.19^{***}
	(−39.74, −38.23)	(−38.95, −36.32)	(−22.76, −22.08)	(−2.1, −1.78)	(−7.31, −4.47)	(−0.2, −0.18)
Langfang	-5.01^{***}	2.94	-11.73^{***}	-3.55^{***}	-35.34^{***}	-0.07^{***}
	(−6.46, −3.57)	(1.54, 4.33)	(−12.29, −11.17)	(−3.95, −3.16)	(−38.38, −32.31)	(−0.08, −0.05)
Qinhuangdao	-21.95^{***}	-25.07^{***}	-23.75^{***}	-6.31^{***}	11.4	-0.22^{***}
	(−23.68, −20.22)	(−26.58, −23.55)	(−24.24, −23.25)	(−6.51, −6.12)	(10.5, 12.3)	(−0.24, −0.2)
Shijiazhuang	-19.16^{***}	-18.55^{***}	-18.7^{***}	-1.75^{***}	-22.15^{***}	-0.27^{***}
	(−20.78, −17.53)	(−20.34, −16.76)	(−19.51, −17.88)	(−1.92, −1.58)	(−25.89, −18.42)	(−0.29, −0.24)

5.1 | Absolute and relative effects in the 68 cities

The COVID-19 lock-down effects $\hat{\tau}$ for the 68 cities in North China on the six pollutants are reported in Table 2 along with their statistical significance levels and confidence intervals by applying the procedure outlined in Section 4. The relative COVID-19 lock-down effects to the potential air pollution levels without COVID-19 event are $\hat{\tau}/\hat{\mu}(0)$ displayed geographically in Figure 5.

Table 2 shows that the COVID-19 control measures significantly decreased concentrations of all six pollutants in the majority of the cities. The effects were the most significant on NO_2 with 67 out of 68 cities having significant reductions at the 5% level, followed by $PM_{2.5}$ (60 cities) and PM_{10} (48 cities), and then CO and O_3 in 51 and 47 cities, respectively. SO_2 exhibited significant COVID-19 effects in 40 cities, which was the least among the six species.

While the reduction in NO_2 and $PM_{2.5}$ were widely spread, Figure 5 shows that the north and east of Shandong province, southwest Hebei and north-central of Henan provinces, and east of Shaanxi had the highest percentages of NO_2 reduction. The high reduction region for $PM_{2.5}$ had some overlap with that of NO_2, which was largely in north Henan, east Shandong, and the city of Tianjin. The effects among different regions show strong heterogeneity, which is related to different air pollution situations. For example, the COVID-19 lock-down effects on $PM_{2.5}$ and NO_2 were much less obvious in the north of Hebei province in comparison to that in the south of Hebei. This is because the concentrations of air pollutants in the cities located in the north of Hebei are much lower than the southern area due to lower industrial emission and more favorable geographical conditions for dispersion of pollutants (Yan et al., 2018), and hence there is less room for further reduction.

The regions with less significant effects on SO_2 were largely located in Shaanxi and Shanxi provinces plus the city Tianjin, and the northwest corner of Hebei province. The coal-firing power plants and domestic heating are major sources

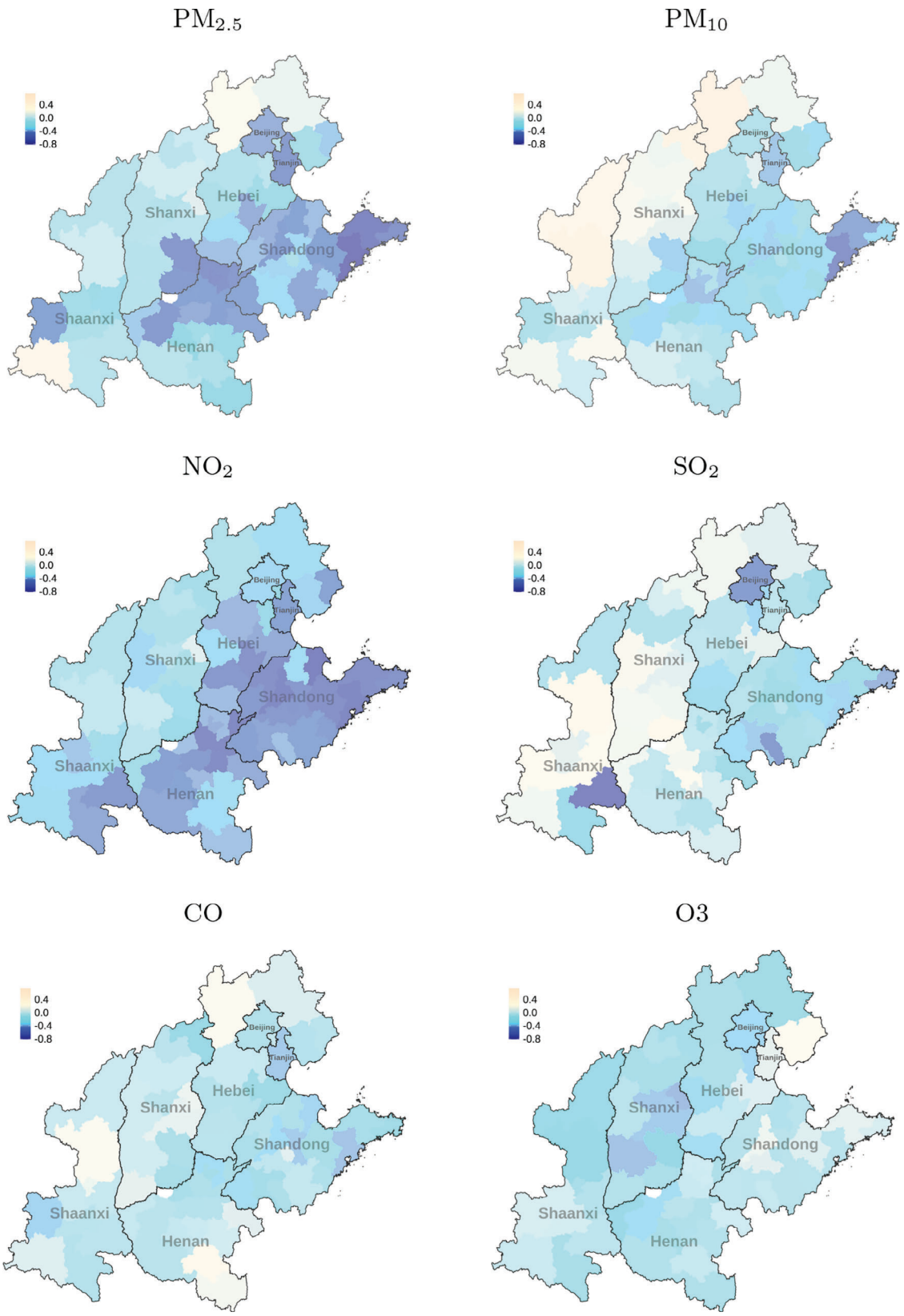

FIGURE 5 Relative changes caused by COVID-19 control measures for the six pollutants, that is, the proportion of effects $\hat{\tau}$ to the potential concentration $\hat{\mu}(0)$ in the absence of COVID-19, shown on maps of the five North China provinces (Hebei, Shandong, Henan, Shanxi and Shaanxi) plus Beijing and Tianjin

TABLE 3 The average COVID-19 effects of the six pollutants: the absolute effects and the relative effects averaged over the cities with significant decreasing effects (middle panel) and all 68 cities (right panel)

	Aggregated on significant cities		Aggregated on all cities	
Pollutant	**Average effects**	**Effects in percentage**	**Average effects**	**Effects in percentage**
$PM_{2.5}$	−34.2 (0.98)	−35.9% (0.70%)	−29.8 (0.87)	−30.9% (0.68%)
PM_{10}	−29.2 (0.96)	−27.6% (0.97%)	−17.8 (0.90)	−14.3% (1.02%)
NO_2	−17.2 (0.39)	−40.3% (0.57%)	−16.9 (0.36)	−39.6% (0.54%)
SO_2	−4.1 (0.16)	−25.0% (0.85%)	−1.7 (0.18)	−10.0% (0.91%)
CO	−0.26 (0.01)	−20.4% (0.69%)	−0.19 (0.01)	−13.9% (0.62%)
O_3	−18.2 (0.94)	−22.9% (1.05%)	−13.3 (0.85)	−16.3% (0.93%)

Note: The units for CO is mg/m^3 and $\mu g/m^3$ for other pollutants. The numbers in the parentheses are the standard errors of the effects calculated via the bootstrap resampling of all the 68 cities.

of SO_2 and CO, which had to be operational during the wintry COVID-19 pandemic period under study. As CO is also a by-product of vehicle emissions, the COVID-19's reducing effect on vehicle travel offers some reduction in CO, which made CO being more significant than SO_2.

Table 3 reports the average amount of absolute and relative reductions for the six pollutants for the 68 cities and those significant cities, with the standard errors calculated via bootstrap resampling after we engage on the temporal block bootstrap to capture the temporal dependence. That NO_2 was the most responsive to the COVID-19 control measures was also reflected in its registering 39.6% reduction relative to the non-COVID-19 baseline $\hat{\mu}_0$ among the 68 cities, followed by $PM_{2.5}$ (30.9%), O_3 (16.3%), PM_{10} (14.3%), CO (13.9%), and SO_2 (10.0%). SO_2 had the least percentages of reductions among the 68 cities.

That NO_2 having the most COVID-19 reductions reflects the fact that the enforced home quarantine in the population had significantly cut down vehicle travel and the related emissions. It is noted that most of the air quality monitoring sites are located in city centers which largely measure NO_2 emissions from the domestic vehicle traffic. The results are consistent with the satellite image data by NASA and the European Space Agency, which showed a dramatic drop in nitrogen dioxide emissions in major Chinese cities compared with the same periods a year earlier (National Aeronautics and Space Administration, 2020).

Part of the CO and O_3 reduction can be attributed to the reduced vehicle travel, as CO and NO_x are concurrent discharge from vehicles, and both NO_2 and O_3 are derivatives of NO_x. The reduction in $PM_{2.5}$ and PM_{10} can be partly attributed to the reductions in NO_2, CO, and SO_2, as the secondary inorganic aerosol is among the highest contributing sources for particulate matters in China (Zhu et al., 2018). That SO_2 being the least significant species is due to that the essential domestic winter heating and power generation had to be operational, and more analyses on SO_2 are given in Supplementary based on data of coal consumption and industrial output.

5.2 | Comparison with the results of raw differences

Existing studies in evaluating the COVID-19's effects on air quality tend to estimate the effects by directly comparing different periods across years or before/during the lock-down, among which the study region of Shi and Brasseur (2020) covers the northern China and shares the most overlap with us. Shi and Brasseur (2020) compared the average concentrations of $PM_{2.5}$, NO_2, O_3 between the period before lockdown (1–22 January) and during the lockdown (23 January to 29 February). They concluded that $PM_{2.5}$ and NO_2 have decreased by 35% and 60%, respectively, and the O_3 has increased by a factor 1.5–2. Our results show that the decrease of $PM_{2.5}$ and NO_2 are at a smaller range 30.9% and 39.6%, and O_3 was also decreased by 16.3% on average. The prominent divergence on the conclusion for O_3 is because Shi and Brasseur (2020) mixed the COVID-19 lock-down effect and the temperature/radiation effect on O_3 as higher temperature and more solar radiation in the lock-down period makes O_3 generation more efficient. We replicate the same calculation for the 68 cities in 2019 over the same temporal design and found there was also an average factor 1.92 of increase over the same two periods in 2019 although there were no policy interventions back then (more

TABLE 4 Comparison between our proposed method and the method of comparing raw averages using (2019, 2) period as contrast ("contrast 2019") and (2020, 1) period as contrast ("contrast prelockdown")

	Effect			Effect in percentage		
Pollutant	Our method	Contrast 2019	Contrast prelockdown	Our method	Contrast 2019	Contrast prelockdown
$PM_{2.5}$	−29.82	−47.72	−29.32	−30.9%	−39.5%	−29.8%
PM_{10}	−17.80	−58.34	−39.69	−14.3%	−37.0%	−29.8%
NO_2	−16.93	−22.89	−28.92	−39.6%	−46.9%	−53.7%
SO_2	−1.74	−8.04	−6.05	−10.0%	−32.6%	−29.7%
CO	−0.19	−0.42	−0.43	−13.9%	−27.4%	−28.5%
O_3	−13.27	9.02	33.49	−16.3%	18.7%	125.5%

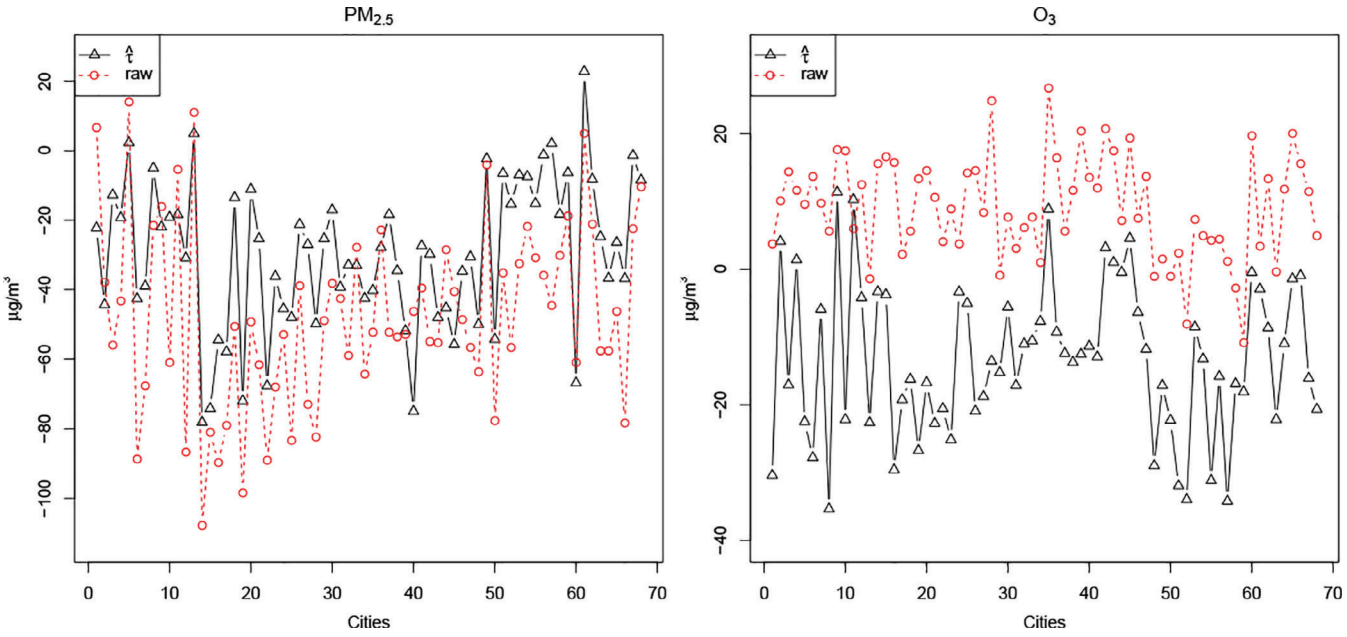

FIGURE 6 The estimated COVID-19 effects $\hat{\tau}$ for $PM_{2.5}$ and O_3 by using the proposed method and differences of the raw averages in Period 2 (shown in Table 1) between 2019 and 2020 for all the cities

details in the SM), which suggests that such an increase tend to be a seasonal variation instead of the effect of the policy.

To display more comparable results calculated on the same dataset, we implemented the direct comparison method on our data of 68 cities. Table 4 compared the results of our method and two simple methods by using the prelockdown period in 2020 and the same period in 2019 as contrast, respectively, where both of the naive methods tend to overestimate the decreasing effects on $PM_{2.5}$, PM_{10}, NO_2, SO_2, CO while lead to increasing effect on O_3.

Figure 6 displays the estimated COVID-19 effects $\hat{\tau}$ for $PM_{2.5}$ and O_3 by using 2019 as contrast. The figures for the other pollutants are provided in the SM. We observed that, for $PM_{2.5}$, the naive method tends to overestimate the decreasing effects, which is partly due to the meteorological confounding as shown in Section 2. And for the evaluation of O_3, the simple method would suggest that the control measures for COVID-19 will increase the concentration of O_3 for most cities. Note that the average temperature in 2020 (3.84°C) was much higher than the average 1.56°C in 2019. This indicates that the increase of O_3 was likely due to the increase of temperature rather than the COVID-19 control measures. The added value of our approach is that the proposed method can neutralize the meteorological confounding and offer an objective measure of the COVID-19 effect on the air quality.

5.3 | Conclusions

The COVID-19 control measures have substantially decreased anthropogenic emissions which lead to effects on the air quality. We analyzed the treatment effects caused by COVID-19 control measures by the Difference in Relative-Difference method on the six major air pollutants, which accounts for both the yearly trends and the meteorological confounders. Significant COVID-19 lock-down effects on air pollution associated with all six pollutants were found in a majority of the cities, and with the most profound decreasing effects on NO_2 and $PM_{2.5}$. In contrast to the would-be outcomes without COVID-19 control, the average concentrations of NO_2 and $PM_{2.5}$ were reduced by 39.6% and 30.9%, respectively. Our quantitative evaluation for the effects on six air pollutants provide an insight into the achievability of air quality improvement caused by significant restrictions in emissions characterized by much-reduced vehicle transportation and industrial outputs of key sections.

ACKNOWLEDGMENTS

This research is funded by China's National Key Research Special Program Grant 2016YFC0207701, 2016YFC0207702, and National Natural Science Foundation of China Grants 71532001, 71973005, 71991472, 11701466, and 11971390. Song Xi Chen acknowledges support from LMEQF at Peking University, Bin Guo from Fundamental Research Funds for the Central Universities JBK1806002, and Jing He from Fundamental Research Funds for the Central Universities JBK2102008 and the Joint Lab of Data Science and Business Intelligence at Southwestern University of Finance and Economics.

REFERENCES

Abadie, A. (2005). Semiparametric difference-in-differences estimators. *The Review of Economic Studies*, *72*(1), 1–19.

Angrist, J. D., & Pischke, J. S. (2008). *Mostly harmless econometrics: An empiricist's companion*. Princeton University Press.

Bauwens, M., Compernolle, S., Stavrakou, T., Muller, J. F., Van Gent, J., Eskes, H., Levelt, P. F., van der, A. R., Veefkind, J. P., Vlietinck, J., & Yu, H. (2020). Impact of coronavirus outbreak on NO_2 pollution assessed using tropomi and omi observations. *Geophysical Research Letters*, *47*(11), e2020GL087978.

Cadotte, M. (2020). Early evidence that COVID-19 government policies reduce urban air pollution. https://doi.org/10.31223/osf.io/nhgj3.

Card, D., & Krueger, A. B. (1994). Minimum wages and employment: A case study of the fast-food industry in New Jersey and Pennsylvania. *The American Economic Review*, *84*(4), 772–793.

Chen, L., Guo, B., Huang, J., He, J., Wang, H., Zhang, S., & Chen, S. X. (2018). Assessing air-quality in Beijing-Tianjin-Hebei region: The method and mixed tales of $PM_{2.5}$ and O_3. *Atmospheric Environment*, *193*, 290–301.

Fassó, A., & Finazzi, F. (2013). A varying coefficients space-time model for ground and satellite air quality data over Europe. *Statistica & Applicazioni*(Special Online Issue), 45–56.

Härdle, W. (1990). *Applied nonparametric regression*. Cambridge University Press.

Lechner, M. (2011). The estimation of causal effects by difference-in-difference methods. *Foundations and Trends in Econometrics*, *4*(3), 165–224.

Liang, X., Zou, T., Guo, B., Li, S., Zhang, H., Zhang, S., Huang, H., & Chen, S. X. (2015). Assessing Beijing's $PM_{2.5}$ pollution: Severity, weather impact, APEC and winter heating. *Proceedings of the Royal Society A: Mathematical, Physical and Engineering Sciences*, *471*(2182), 20150257.

Liu, H., Ye, F., Sun, H., Guo, B., Liu, R., Xiao, J., He, J., Zheng, X., Wang, H., & Chen, S. X. (2019). *Air quality assessment report 6, results on 2+43 cities from 2013 to 2018, Technical report*. Peking University, China.

Lu, C., Nie, X. & Wager, S. (2019). Robust nonparametric difference-in-differences estimation. *arXiv:1905.11622*.

Ministry of Ecology and Environment of China (2018). 2018-2019 action plan for the air pollution prevention and management for the fen-wei plain. Retrieved from http://www.mee.gov.cn/xxgk2018/xxgk/xxgk03/201810/t20181029_667650.html

National Aeronautics and Space Administration (2020). Airborne nitrogen dioxide plummets over China. Website. Retrieved from https://earthobservatory.nasa.gov/images/146362/airborne-nitrogen-dioxide-plummets-over-China

Otmani, A., Benchrif, A., Tahri, M., Bounakhla, M., El Bouch, M., & Krombi, M. (2020). Impact of COVID-19 lockdown on PM_{10}, SO_2 and NO_2 concentrations in salé city (Morocco). *Science of the Total Environment*, *735*, 139541.

Rubin, D. B. (1974). Estimating causal effects of treatments in randomized and nonrandomized studies. *Journal of Educational Psychology*, *66*(5), 688–701.

Sharma, S., Zhang, M., Gao, J., Zhang, H., Kota, S. H., et al. (2020). Effect of restricted emissions during COVID-19 on air quality in india. *Science of the Total Environment*, *728*, 138878.

Shen, H., Tao, S., Chen, Y., Ciais, P., & Zhao, S. (2017). Urbanization-induced population migration has reduced ambient $PM_{2.5}$ concentrations in China. *Science Advances*, *3*(7), e1700300.

Shi, X., & Brasseur, G. (2020). The response in air quality to the reduction of chinese economic activities during the COVID-19 outbreak. *Geophysical Research Letters*, *47*(11), e2020GL088070.

Sicard, P., De Marco, A., Agathokleous, E., Feng, Z., Xu, X., Paoletti, E., Rodriguez, J. J. D., & Calatayud, V. (2020). Amplified ozone pollution in cities during the COVID-19 lockdown. *Science of the Total Environment*, *735*, 139542.

Simonoff, J. S. (2012). *Smoothing methods in statistics*. Springer Science & Business Media.

State Council of China (2013). Atmospheric pollution prevention and control action plan, Website. Retrieved from http://www.mee.gov.cn/home/ztbd/rdzl/dqst/201307/t20130709_255093.shtml

Tan, Z., Lu, K., Dong, H., Hu, M., Li, X., Liu, Y., Lu, S., Shao, M., Su, R., Wang, H., Wu, Y., Wahner, A., & Zhang, Y. (2018). Explicit diagnosis of the local ozone production rate and the ozone-nox-voc sensitivities. *Science Bulletin*, *63*(16), 1067–1076.

Tânia, F., Peilin, L., Nelson, B., & Zhao, P. (2017). Trends of $PM_{2.5}$ concentrations in China: A long term approach. *Journal of Environmental Management*, *196*, 719–732.

Wan, Y., Xu, M., Huang, H., & Chen, S. X. (2021). A spatio-temporal model for the analysis and prediction of fine particulate matter concentration in Beijing. *Environmetrics*, *32*(1), e2648.

Wang, P., Guo, H., Hu, J., Kota, S. H., Ying, Q., & Zhang, H. (2019). Responses of $PM_{2.5}$ and O_3 concentrations to changes of meteorology and emissions in China. *Science of the Total Environment*, *662*, 297–306.

Yan, D., Lei, Y., Shi, Y., Zhu, Q., Li, L., & Zhang, Z. (2018). Evolution of the spatiotemporal pattern of $PM_{2.5}$ concentrations in china–A case study from the Beijing-Tianjin-Hebei region. *Atmospheric Environment*, *183*, 225–233.

Zhang, S., Chen, S. X., Guo, B., Wang, H. & Lin, W. (2020), 'Regional air-quality assessment that adjusts for meteorological confounding', *Science China, Mathematics (in Chinese) 50*(4), 527–558. The English translation is available from https://doi.org/10.1360/SCM-2019-0368.

Zhu, Y., Huang, L., Li, J., Ying, Q., Zhang, H., Liu, X., Liao, H., Li, N., Liu, Z., Mao, Y., & Fang, H. (2018). Sources of particulate matter in China: Insights from source apportionment studies published in 1987–2017. *Environment International*, *115*, 343–357.

SUPPORTING INFORMATION

Additional supporting information may be found online in the Supporting Information section at the end of this article.

How to cite this article: Zheng X, Guo B, He J, Chen SX. Effects of corona virus disease-19 control measures on air quality in North China. *Environmetrics*. 2021;e2673. https://doi.org/10.1002/env.2673